PCCP

Accepted Manuscript

This article can be cited before page numbers have been issued, to do this please use: P. Berton, S. P. Kelley, H. Wang, A. S. Myerson and R. D. Rogers, *Phys. Chem. Chem. Phys.*, 2017, DOI: 10.1039/C7CP04078D.

ROYAL SOCIETY OF CHEMISTRY

rsc.li/pccp

View Article Online
DOI: 10.1039/C7CP04078D

Journal Name

ARTICLE

Separate Mechanisms of Ion Oligomerization Tune the Physicochemical Properties of n-Butylammonium Acetate: Cation-Base Clusters *vs.* Anion-Acid Dimers

Received 00th January 20xx,
Accepted 00th January 20xx

DOI: 10.1039/x0xx00000x

www.rsc.org/

Paula Berton,[a] Steven P. Kelley,[a] Hui Wang,[b] Allan S. Myerson,[c] and Robin D. Rogers[a,d]

We investigated the ability of the ions comprising protic ionic liquids to strongly interact with their neutral acid and base forms through the characterization of n-butylammonium acetate ([C_4NH_3][OAc]) in the presence of excess n-butylamine (C_4NH_2) or excess acetic acid (HOAc). The conjugate and parent acid or base form new nonstoichiometric noncovalently bound species (*e.g.*, oligomeric ions) which change the physical and chemical properties of the resulting liquids, thus offering tunability. The effects of adding C_4NH_2 or HOAc to [C_4NH_3][OAc] on the resulting thermal and spectroscopic properties differ and suggest that C_4NH_2 interacts primarily with $[C_4NH_3]^+$ to form 3-dimensional polymeric networks likely similar to those in $H_2O/[H_3O]^+$, while HOAc interacts primarily with $[OAc]^-$ to form oligomeric ions (*e.g.*, $[H(OAc)_2]^-$). The densities of the systems increased with increase of acid content and reached a maximum when the acid molar fraction was 0.90, but decreased with increased amine concentration. The viscosities decreased significantly with increasing acid or base concentration. The solvent properties of the mixtures were assessed by measuring the solubilities of benzene, ethyl acetate, diethyl ether, heptane, ibuprofen free acid, and lidocaine free base. The solubilities of the organic solutes and APIs can be tuned with the concentration of acid or amine in the mixtures. In addition, crystallization of the active pharmaceutical ingredients can be induced with the modification of the composition of the mixtures. These observations support the usage of these mixtures for the synthesis and purification of acid or basic active pharmaceutical ingredients in the pharmaceutical industry.

Introduction

The use of ionic liquids (ILs, defined as liquids composed entirely of ions with melting points up to 100 °C[1]) in liquid-based separation processes has been heavily explored as a result of the concept that their physicochemical properties are tunable depending on the ions that compose them.[2,3] An even more diverse and tunable array of liquids can be prepared by mixing different ILs,[4] dissolving higher melting salts in ILs,[5,6] or chemical reactions that produce mixtures of ions.[7] We term these systems double salt ionic liquids (DSILs)[8] because, like crystalline double salts, they involve ionic bonds between one ion to two (or more) chemically distinct counterions. Using DSILs as proof of concept, we were able to show how different properties, such as hydrogen-bond basicity[9] and hydrophobicity, could be affected by the formation of new species in the DSIL which are not possible to form in the starting salt.[10,11]

In our continuing research to expand the range of solvent properties possible with ILs, we decided to explore protic ILs. The key properties that distinguish protic ILs from other ILs relate to the proton transfer from an acid to a base, leading to the presence of proton-donor and -acceptor sites, which can be used to build up a hydrogen-bonded network and modify the physical and chemical properties of the systems.[12,13] The systems can further be changed by adding excess amounts of acid or base, which was shown when acetic acid (HOAc) in *N*-methylpyrrolidine-HOAc mixtures were reported to increase the ionicity of the system, due to the presence of oligomeric anionic species $[(OAc)_xH_{x-1}]^-$, stabilized by hydrogen bonds.[14]
Our group has explored strategies for changing the physical properties of active pharmaceutical ingredients (APIs) without covalent modification by making protic API-based ILs including tetrabutylammonium salts of oligomeric ions based on salicylate/salicylic acid in presence of tetrabutylphosphonium[15] and low melting, partially ionized systems composed of lidocaine or salicylic acid added to lidocainium salicylate.[15] In addition, protic ILs of ethanolamines and fatty acids, which form liquid crystals, are capable of melt congruently with their parent acid or amine to generate new lyotropic phases, showing that even the structure of mesophases is affected by ion oligomerizaiton.[16] Given the vast range of acids and bases which can be incorporated into ILs, examples like these are just a small fraction of a largely unexplored realm of complex, high-ionicity liquids.

[a] *Department of Chemistry, McGill University, 801 Sherbrooke St. West, Montreal, QC H3A 0B8, Canada.*
[b] *Institute of Process Engineering, Chinese Academy of Sciences, Beijing 100190, China.*
[c] *Novartis-MIT Center for Continuous Manufacturing and Department of Chemical Engineering, Massachusetts Institute of Technology, Cambridge, MA 02139, USA.*
[d] *525 Solutions, Inc., 720 2nd Street, Tuscaloosa, AL 35401, USA.*
Electronic Supplementary Information (ESI) available: Thermal analysis, Spectroscopic data. See DOI: 10.1039/x0xx00000x

View Article Online
DOI: 10.1039/C7CP04078D

It is well known that proton transfer in a protic IL is reversible and that the ratio of ionized to neutral species can be tuned both by selection of the acid-base pair[17] and changing the acid-base ratio.[18] The characterization and classification of such ILs frequently consist of treating them as mixtures of ionized and non-ionized species in various proportions.[19] These methods are useful for understanding certain properties of ILs which depend explicitly on the concentration of ions, particularly vapor pressure and conductivity.[20] However, we believe many other properties of protic ILs such as mass transport, dissolving power, and crystallization kinetics, are better understood through the DSIL approach, which recognizes that such systems are affected by new species held together by noncovalent forces which may only be possible to form in the mixture.

In this study, we apply such an approach to the characterization of systems composed of n-butylammonium acetate ($[C_4NH_3][OAc]$), with excess acetic acid (HOAc) or n-butylamine (C_4NH_2, mentioned as "butylamine" in the following). $[C_4NH_3][OAc]$ is of technical relevance as a low-melting salt (mp 48 °C) which is itself made from two common solvents and, furthermore, shows variable ionicity even as a neat compound. Physical properties, including density and viscosity, of the mixtures were measured, and excess molar volumes were calculated based on density data. To evaluate the chemical properties, the solubilities of various organics (ethyl acetate, heptane, diethyl ether, and benzene) and pharmaceuticals (ibuprofen and lidocaine) in the mixtures were determined. Interactions between the species in the mixtures, as well as the physicochemical property behaviors are discussed based on thermogravimetric and spectroscopic data.

Experimental

Chemicals

Glacial HOAc was purchased from Fischer Scientific (Hampton, NH). Benzene (HPLC grade), C_4NH_2, and sodium ibuprofen ([Na][Ibu]) were obtained from Sigma-Aldrich (Milwaukee, WI). Ethyl acetate, heptane, and hydrochloric acid were obtained from Sigma-Aldrich (St. Louis, MO). Diethyl ether was supplied by EMD Chemicals, Inc. (Gibbstown, NJ). Lidocaine was supplied by Spectrum Chemical Mfg. Corp. (Gardena, CA). Deuterated chloroform ($CDCl_3$) and dimethyl sulfoxide (DMSO-d_6) were purchased from Cambridge Isotope Laboratories, Inc. (Andover, MA). All solvents and reagents were used as received unless specified. Deionized (DI) water was obtained from a commercial deionizer (Culligan, Northbrook, IL) with specific resistivity of 17.30 MΩ cm at 25 °C.

Synthesis of n-Butylammonium Acetate

Synthesis of $[C_4NH_3][OAc]$ followed our previous procedure.[21] Briefly, 0.105 mol C_4NH_2 was placed in a 50 mL round bottom flask. The flask was cooled to 0 °C using an ice-water bath while stirring vigorously with a magnetic stir bar. Glacial HOAc (0.1 mol) was added dropwise to C_4NH_2 while maintaining the temperature at 0 °C, as the reaction was exothermic. The solution was stirred for 24 h while remaining in the water bath, but the temperature was allowed to slowly rise to ambient conditions. Then, the excess amine was removed using rotary evaporation, and the IL was washed with 20 mL diethyl ether for three times (20 mL × 3) to remove any remaining starting materials. The final obtained IL was dried under high vacuum at room temperature with magnetic stirring for 12 h to remove any volatiles as much as possible. Purity and composition were confirmed using NMR.

Alternatively, $[C_4NH_3][OAc]$ could be isolated without washing using the following procedure. The reactants were combined and reacted as described above. The resulting liquid was crystallized by adding a seed crystal of $[C_4NH_3][OAc]$ or octylammonium acetate ($[C_8NH_3][OAc]$) at room temperature. Crystalline $[C_4NH_3][OAc]$ was separated from liquid impurities by centrifugation at 10,000 rpm for *ca.* 1 min in a VWR Micro 1207 centrifuge (VWR International, Radnor, PA).

Preparation of the Mixtures

The $[C_4NH_3][OAc]$ and HOAc (or C_4NH_2) mixtures were prepared as *ca.* 1 g samples, by mass addition of the corresponding amounts of IL and HOAc (or C_4NH_2) with molar fraction of HOAc (or C_4NH_2), χ, at 0.10, 0.20, 0.33, 0.50, 0.67, 0.80, and 0.90. Each system was stirred thoroughly for 1 h and stored in a desiccator.

Synthesis of Ibuprofen Free Acid

15 mmol [Na][Ibu] was dissolved in 20 mL DI water. HCl solution (2 M, 7.5 mL, containing 15 mmol HCl), was added dropwise to the [Na][Ibu] solution. The mixture was stirred at room temperature for 2 h. The produced ibuprofen was not soluble in water and precipitated from the solution. The precipitate was separated by filtration using house vacuum, washed with DI water twice (100 mL × 2), and oven-dried (Precision Econotherm Laboratory Oven, Natick, MA) at 65 °C for 72 h (mp: 74.2 °C). (^{1}H NMR (500 MHz, DMSO-d_6): 12.26 (s, 1H); 7.18 (d, 2H); 7.12 (d, 2H); 3.64 (q, 1H); 2.41 (d, 2H); 1.82 (m, 1H); 1.36 (d, 3H); 0.87 (d, 6H).)

Single Crystal and Powder X-Ray Diffraction

Single crystal X-ray diffraction (SCXRD) data was collected on a Bruker D8 Venture diffractometer equipped with a Photon 100 CMOS area detector and a dual-anode IμS microfocus X-ray source (Bruker AXS, Madison, WI). Crystals were isolated under an optical polarizing microscope and mounted on a glass fiber using heavy hydrocarbon oil (Hampton Research, Aliso Viejo, CA). A hemisphere of data was collected for each crystal using a strategy of scans about omega and phi with 0.5° frame widths. Data collection, integration, and absorption corrections were performed using the Apex3 software (Bruker AXS)[22] and SADABS.[23] Structure solution and refinement were conducted using the SHELX v. 2013[24] software package from Bruker. Packing diagrams for the structure were made using Mercury (Cambridge Crystallographic Data Center (CCDC), Cambridge, UK).[25] Non-hydrogen atoms in the structure were located from the difference map and refined an isotropically through least squares refinement against F^2. Hydrogen atoms bonded to nitrogen were located from the difference map, their coordinates were refined freely, and their thermal parameters were constrained to ride on the carrier atom. Hydrogen atoms bonded to carbon were placed in calculated positions and

allowed to ride on the carrier atom. Hydrogen atoms on methyl groups were refined using a riding rotating model.

Powder X-ray diffraction (PXRD) was measured on a Bruker D8 Advance diffractometer equipped with a Lynxeye linear position sensitive detector. $[C_4NH_3][OAc]$ was loaded into a 0.5 mm capillary and analyzed in transmission geometry across a 2-theta range of 6-50° using a scanning rate of 4 s/0.02°. The sample was rotated about the phi axis at 15 rpm, corresponding to one full rotation per step.

Thermal Analysis

Thermal gravimetric analysis (TGA) was performed using a Discovery TGA 5500 system (TA Instruments, New Castle, DE) under nitrogen. Samples, between 5 and 10 mg, were placed in aluminum pans and heated from 40 to 600 °C at a heating rate of 5 °C/min, with an isotherm at 75 °C for 30 min, to eliminate any volatiles.

Differential scanning calorimetry (DSC) was performed using a Discovery DSC 2500 unit (TA Instruments) under nitrogen to determine thermal transition temperatures. Samples between 5 and 15 mg were placed in hermetically sealed aluminum pans, and the following protocols were followed. For liquids, samples were cooled from 25 to -90 °C at a cooling rate of 5 °C/min with an isotherm at -90 °C of 10 min, and then heated to 25 °C heating rate of 5 °C/min with an isotherm at 25 °C of 5 min. The cooling/isotherm/heating/isotherm steps were repeated two more times (three cycles in total). Crystals of pure $[C_4NH_3][OAc]$ (solid) were heated first to 60 °C, heating rate of 5 °C/min with an isotherm at 25 °C of 5 min, and then cooled to -90 °C, cooling rate of 5 °C/min with an isotherm at -90 °C of 10 min. The heating/isotherm/cooling/isotherm steps were repeated two more times (three cycles in total).

Spectroscopic Determinations

^{1}H NMR spectra were taken utilizing a 500 MHz Bruker Avance NMR spectrometer (Karlsruhe, Germany). Pure C_4NH_2, HOAc, $[C_4NH_3][OAc]$, and the mixtures were loaded solventless in a flame-sealed capillary, and the spectra were collected at 25 °C using $CDCl_3$ as the external lock. The solutions saturated by ethyl acetate, benzene, heptane, diethyl ether, ibuprofen, or lidocaine were dissolved in $CDCl_3$ and ^{1}H NMR spectra were collected at 25 °C.

Infrared spectroscopic measurements of C_4NH_2, HOAc, $[C_4NH_3][OAc]$, and the mixtures were taken on neat samples by utilizing an Attenuated Total Reflectance-Fourier Transform Infrared (ATR-FTIR) spectrometer (Bruker Alpha, Billerica, MA), allowing for direct observation of the liquids. Spectra were obtained in the range of ν_{max} = 400–4000 cm^{-1}.

Water Content, Density, and Viscosity Measurements

Water contents of HOAc, C_4NH_2, $[C_4NH_3][OAc]$, and the mixtures were measured with a Karl Fischer titrator (Mettler Toledo C20 coulometric KF) using AQUASTAR CombiCoulomat fritless methanol solution as the titrant (Merck, Whitehouse Station, NJ). Samples were loaded into syringes, tared, and injected into the KF titrator through a sealed septum. The sample mass was determined by difference weighing. Titration and water content calculations were performed automatically by the titrator.

Density measurements were taken using an Anton-Paar DMA 500 density meter (Ashland, VA) at 30 °C (±0.1 °C) by filling 1 mL of each sample into the measuring cell. Measurement repeatability was 0.0002 g/cm^3. The viscosities were measured using a Cambridge Viscosity Viscometer (VISCOlab 3000, Medford, MA). Approximately 1 mL of each sample was placed in the sample chamber. The correct sized piston corresponding to the expected viscosity range was used and the measurement was taken at 30 °C.

Organics and Drug Solubility Measurement

The solubilities of heptane, diethyl ether, ethyl acetate, and benzene in the mixtures were determined by adding the organics drop by drop to 0.5 g of each sample. If the solution was still clear when the molar ratio of the organic solvent to the IL mixture reached 25:1, the IL mixture and organic solvent were considered to be totally miscible. If a turbid solution was obtained after adding one more drop of the organic solvent, the IL mixture was saturated and the solutions were analyzed by ^{1}H NMR. The molar ratios of solute/$[OAc]^-$ for the mixtures of $[C_4NH_3][OAc]$ and HOAc (or the solute/$[C_4NH_3]^+$ for the mixtures of $[C_4NH_3][OAc]$ and C_4NH_2) were calculated through direct integration of appropriate signals.[26]

The solubility of ibuprofen in the mixtures of $[C_4NH_3][OAc]$ and HOAc (or C_4NH_2) was tested by loading 0.05 g free ibuprofen into a vial loaded with 0.5 g of each mixture and stirring. If all the added ibuprofen was dissolved, an additional amount was added until no more could dissolve, indicating the solvent was saturated. The solution was then separated from the particulate matter using a PTFE syringe filter with pore size of 0.45 µm. The concentrations of ibuprofen in the saturated solutions were determined by dissolving each solution in $CDCl_3$ and analyzed by ^{1}H NMR, and the ibuprofen/$[OAc]^-$ (or C_4NH_2) molar ratios were calculated through direct integration of appropriate signals. Solubility of lidocaine in the mixtures of $[C_4NH_3][OAc]$ and C_4NH_2 (or HOAc) followed a similar procedure as that for ibuprofen solubility in the mixtures.

Results and Discussion

Synthesis, crystallization, and crystal structure of $[C_4NH_3][OAc]$

The IL $[C_4NH_3][OAc]$ was prepared following the procedure previously reported.[21] In summary, glacial HOAc was added dropwise to neat C_4NH_2 at 0 °C and with continuous stirring, giving a colorless liquid which, within 30 min of addition, became highly viscous at 0 °C (Experimental, Section 2.2). The resulting IL was stored for up to 3 days at room temperature in a closed flask but showed no crystallization. However, when part of the resulting liquid was ground with a seed crystal of $[C_8NH_3][OAc]$, it completely solidified to give a white powder. The rest of the liquid could be solidified by adding a small amount of this powder. The solid could be partially melted and recrystallized multiple times by heating it in a sealed container using a heat gun. Milligram quantities of crystals exposed to ambient atmosphere were found to liquefy within a few minutes, although it should be noted that addition of $[C_4NH_3][OAc]$ or $[C_8NH_3][OAc]$, grinding with the seed crystal,

View Article Online
DOI: 10.1039/C7CP04079D

and transferring the melt from one container to another were all done under open atmosphere and did not stop the bulk from crystallizing.

One of the large crystals obtained from the melting and recrystallizing process described above was analyzed by SCXRD (Fig. 1*b*) and identified as the 1:1 salt $[C_4NH_3][OAc]$, which crystallized in $P2_1/c$ with one unique formula unit . The cation is in an all-*transoid* configuration, and the three hydrogen atoms bonded to nitrogen were located from the difference map and refined to give the expected tetrahedral geometry around the nitrogen atom. The acetate C-O bond distances are close but asymmetric (1.257(3) *vs.* 1.265(3) Å). The oxygen which forms longer bond engages in more strong hydrogen bonds than the other oxygen atom. The packing is grossly similar to the other two structurally characterized $[C_nNH_3][OAc]$, n= 6 or 8.[21] The PXRD spectra of the bulk solid (measured at ambient temperature, Fig. 1*c*) matches that of the simulated spectrum from the crystal structure (measured at 0 °C), confirming $[C_4NH_3][OAc]$ is the only detectable solid phase (*i.e.,* no crystalline hydrates or off-stoichiometry solids were formed).

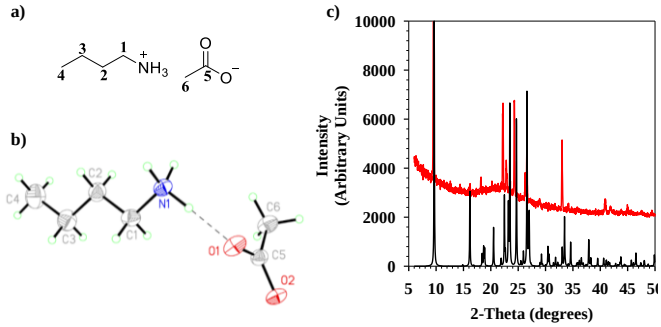

Figure 1. a) Structure of $[C_4NH_3][OAc]$; **b)** Labeled 50% probability ellipsoid plot of formula unit of $[C_4NH_3][OAc]$ (dashed line indicates shortest contact between ions); and **c)** Measured (red) *vs.* calculated (black) PXRD diffractograms for $[C_4NH_3][OAc]$.

The crystal structure is consistent with a fully ionized salt. It is known that there is a strong correlation between proton transfer from the acid to the base and the pKa difference (ΔpK_a) between the acid and base precursors. In the selected protic IL, the pK_a of C_4NH_2 and HOAc are 10.8 and 4.8, respectively, resulting in a ΔpK_a of 6. Since the ΔpK_a is higher than 4, full ionization is likely, although ILs can have detectible quantities of neutral acid and base for pK_a differences as large as 10.[27]

The 1:1 salt is a well ordered ionic compound in the crystalline state (mp: 46.4 °C, DSC, Fig. S1, ESI) and, after melting, it is easily supercooled to its glass transition. It is possible that prior to crystallization, the liquid may contain nonionized and ionized species, even though the solid is apparently fully ionized, and this may be responsible for inhibition of the crystallization. Such an effect has been observed in other systems; for instance, salts of the hydrogen succinate anion can disproportionate into neutral succinic acid and succinate dianions resulting in more complex structures than expected from the stoichiometry.[28] This has been invoked to explain the exceptionally low melting point of hydrogen succinate ILs.[29]

The crystal structure suggested to us that we could disrupt the well-ordered nature of the 1:1 salt by adding more hydrogen-bond donors or acceptors. To test our hypothesis, we added HOAc or C_4NH_2 to the liquid $[C_4NH_3][OAc]$ at different molar ratios (χ), up to χ = 1. The prepared mixtures were all liquids. In contrast to our previous work on DSILs,[10-12] the volatility of C_4NH_2 and HOAc prevented us from drying these mixtures after preparation without changing their composition (TGA, Fig. S2, ESI). However, the water content of each mixture (Table S1, ESI) was below 6000 ppm, in reasonable agreement with those of hydrophilic ILs like 1-ethyl-3-methylimidazolium acetate used in other analytical studies.[30]

Thermal Analysis of the Mixtures

$[C_4NH_3][OAc]$ + HOAc. The DSC traces of the supercooled liquid $[C_4NH_3][OAc]$ showed that it can be reversibly cooled to its glass transition temperature (Fig. 2a.*a*) without crystallizing. At 0.1 molar fraction HOAc, $[C_4NH_3][OAc]$ crystallized on warming during the first cycle (DSC, Fig. S3, ESI) and reversibly liquefies and crystallizes on warming and cooling, respectively, near room temperature (Fig. 2a.*a*). This may be a stochastic event, as 0.2 and 0.33 do not show any new transitions, although the glass-liquid onset on warming is pushed to lower temperatures (Fig. 2a.*b*). At 0.5 molar fraction HOAc, there are exothermic and endothermic events on warming which likely indicate a crystallization (Fig. 2a.*c*) followed by a complex melting process (Fig. 2a.*d*). The level baseline after the final endotherm indicates that the system becomes liquid at a temperature far below the melting points of either $[C_4NH_3][OAc]$ or HOAc, and the transitions are therefore associated with a new crystalline phase. At 0.67 molar fraction HOAc there are no detectable events, while at 0.8 molar fraction there is an exotherm and endotherm that match roughly with those at 0.5 but are broadened (Fig. 2a.*e,* 2a.*f*). These transitions also appear to occur at 0.9 molar fraction HOAc (Fig. 2a.*g*, 2a.*h*, respectively), along with the crystallization (Fig. 2a.*i*) and melting (Fig. 2a.*j*) of pure HOAc. It is interesting to note that the crystallization of HOAc releases far more heat than any transition involving the DSIL species, which reflects how much the DSILs destabilize the crystal structure.

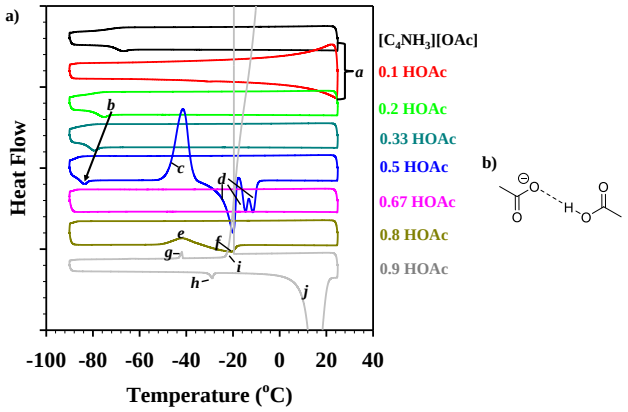

Figure 2. a) 3rd warming and cooling cycles of DSC scans for the mixtures of $[C_4NH_3][OAc]$ + HOAc. Molar fraction HOAc is indicated in the legend. Exothermic transitions are in the +*y* direction (1 tick mark = 0.2 W/g); Letters *a*-*j* refer to assignment described in text. **b)** Schematic of the interaction between $[OAc]^-$ and HOAc to form a discrete oligomeric ion.

The net effect of HOAc appears to be to inhibit crystallization, which is in agreement with studies on deep eutectic solvents made with salts and carboxylic acids[31] and the addition of HOAc

View Article Online
DOI: 10.1039/C7CP04079D

to [C_2mim][OAc] to increase its fluidity by generating oligomeric ions.[14] The sharp transitions at 0.5 (Fig. 2a.*c*, 2a.*d*) and broadened transitions at 0.8 and 0.9 (Fig. 2a.*e*, 2a.*f*, 2a.*g*, 2a.*h*) are consistent with the formation of a new crystalline compound that has a 1:1 ratio of [C_4NH_3][OAc] and HOAc, *e.g.*, $[H(OAc)_2]^-$ (Fig. 2b), which melts in the former case and dissolves in excess HOAc in the latter. The 1:1 adducts of carboxylates with their conjugate acids are quite common and have been crystallographically characterized for $[OAc]^-$ ILs.[32] These oligomeric ions have been shown to lower the melting points and inhibit crystallization of carboxylate salts,[15] and both the lower melting point of the 1:1 compound and the general tendency of the system to crystallize only sporadically are consistent with the formation of such ions.

[C_4NH_3][OAc] + C_4NH_2. The DSC of C_4NH_2 was not recorded due to its high volatility even at room temperature (as reflected in TGA data, Fig. S2, ESI). Adding excess C_4NH_2 to the supercooled liquid [C_4NH_3][OAc] (Fig. 3a.*a*) results in additional new transitions, indicating changes in the organization of the molecules in solution. At 0.1-0.2 molar fraction C_4NH_2, [C_4NH_3][OAc] is able to crystallize on first warming (DSC, Fig. S4, ESI) and begins dissolving and recrystallizing near room temperature on warming and cooling, respectively, as indicated by the diverging baselines (Fig. 3a.*b*). Exothermic transitions are visible in both systems on cooling, becoming more pronounced in 0.2 molar fraction C_4NH_2 (Fig. 3a.*c*) and appear to have corresponding endothermic reverse transitions on warming (Fig. 3a.*d*). Since [C_4NH_3][OAc] is likely crystalline at this point in the DSC, these transitions are reasonably assigned to a more C_4NH_2-rich phase. At 0.33 molar fraction, it is evident from the three separate exothermic events that a new crystalline phase is forming, as [C_4NH_3][OAc] does not undergo solid-solid transitions. The first transition to occur on cooling (Fig. 3a.*e*) is presumably the reverse of the dissolution that begins on second warming (DSC, Fig. S4, ESI), and all other transitions are therefore likely associated with a C_4NH_2-rich phase (Fig. 3a.*f*, 3a.*g*, 3a.*h*).

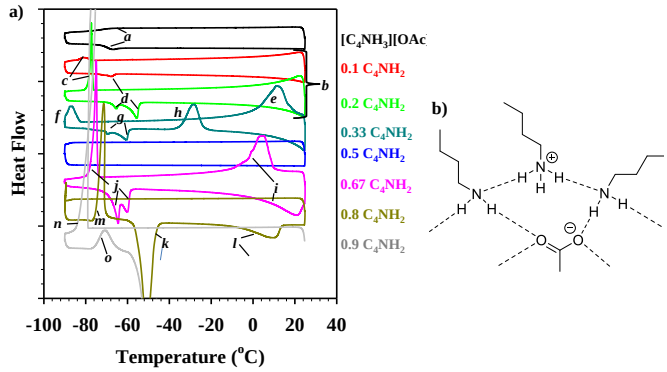

Figure 3. a) 3rd warming and cooling cycles of DSC scans for the mixtures of [C_4NH_3][OAc] + C_4NH_2. Molar fraction of C_4NH_2 is indicated in the legend. Exothermic transitions are in the +*y* direction (1 tick mark = 0.2 W/g); Letters *a*-*o* refer to assignment described in text. **b)** Schematic depicting likely interactions of C_4NH_2 with [C_4NH_3][OAc].

At 0.5 molar fraction C_4NH_2, no transitions are observed in any cycles. Increasing the molar fraction to 0.67 results in a re-appearance of the dissolution and crystallization of [C_4NH_3][OAc] near room temperature (Fig. 3a.*i*) and the exothermic and endothermic transitions associated with the C_4NH_2-rich phase (Fig. 3a.*j*). From 0.8-0.9 molar fraction C_4NH_2, the two endothermic peaks on warming in most other C_4NH_2-containing systems are replaced with a single endotherm which is in agreement with the reported melting point of pure C_4NH_2 (Fig. 3a.*k*), followed by a broad transition which is likely dissolution of [C_4NH_3][OAc] (Fig. 3a.*l*). It appears that C_4NH_2 and [C_4NH_3][OAc] crystallize concomitantly on warming at 0.8 molar fraction (Fig. 3a.*m*) and separately at 0.9, with C_4NH_2 crystallizing on cooling (Fig. 3a.*n*) and [C_4NH_3][OAc] on warming (Fig. 3a.*o*). Also, like HOAc, the transitions involving molecular C_4NH_2 are for more intense than any that involve the IL or DSILs. The DSC curves point to a wide range of effects of C_4NH_2 on the speciation and properties of the IL. Small amounts of C_4NH_2 enable [C_4NH_3][OAc] to crystallize, which may be due to the ability of C_4NH_2 to conduct protons through a Grotthus mechanism. This would not change the net speciation of the system, but would effectively increase the mobility of $[C_4NH_3]^+$ ions and, consequently, the probability of crystallization. Conversely, the ability of [C_4NH_3][OAc] to inhibit the crystallization of C_4NH_2 up to at least 0.67 molar fraction is consistent with the fact that $[C_4NH_3]^+$ can accommodate a large number of hydrogen bond acceptors and suggests that C_4NH_2 displaces $[OAc]^-$. A possible scheme of such an interaction is also shown in Fig. 3b. DSC alone cannot confirm how strongly C_4NH_2 is bound to the other ions in the system and whether there is significant charge transfer, but the effect is at least great enough to allow the formation of new crystalline phases. The apparent generation of new crystalline phases across a wide range of compositions contrasts with the effect of HOAc, where the oligomeric ions suppress crystallization except at very precise, stoichiometric concentrations.

Spectroscopic Characterization of the Mixtures

Nuclear Magnetic Spectroscopy (NMR) was used to understand the interactions between the species in the mixtures complementing the observations using thermogravimetric determinations. ^{1}H NMR spectra were collected by loading the neat samples in capillaries using $CDCl_3$ as external lock and were compared to those of [C_4NH_3][OAc] + HOAc (or C_4NH_2). The full spectra of the [C_4NH_3][OAc] + HOAc mixtures are shown in Fig. S5, ESI (Fig. S7, ESI, for C_4NH_2). The proton chemical shift deviations ($\Delta\delta$) of the mixtures as a function of HOAc concentration were calculated according to eq. (1) and are illustrated in Fig. S6, ESI (Fig. S8, ESI, for C_4NH_2).

$$\Delta\delta = \delta(\text{Mixture}) - \delta([C_4NH_3][OAc]) \quad (1)$$

We have previously used solventless NMR chemical shifts to understand how the chemical environment of a given ion in a DSIL changes as a function of the ratio of its counterions.[10] For this system, however, there is a second effect which must be considered, which is the fact that the signals of C_4NH_2 or HOAc become averaged with their conjugate acids and bases. If the signal was simply due to the weighted combination of the two species, every point would be expected to fall on a straight line connecting the signal from pure HOAc or C_4NH_2 with pure [C_4NH_3][OAc], and deviations from this line can therefore be

interpreted as changes in chemical environment. It can be seen in Fig. 4 that the actual trend is for the Δδ values of all protons to follow a roughly parabolic curve which always falls below the hypothetical straight line, indicating that both C_4NH_2 and HOAc shift their conjugate acid or base upfield. For C_4NH_2, the upfield shift is straightforward as it should act as a base towards $[C_4NH_3]^+$ and donate electron density. HOAc may cause an upfield shift in $[OAc]^-$ because it substitutes cationic $[C_4NH_3]^+$ groups in hydrogen bonds, resulting in less charge transfer away from the $[OAc]^-$.

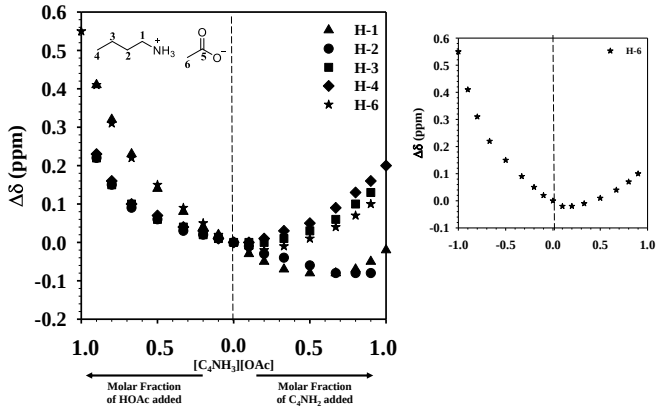

Figure 4. Proton chemical shift deviations (Δδ) of the mixtures of $[C_4NH_3][OAc]$ + HOAc (*left side*) and $[C_4NH_3][OAc]$ + C_4NH_2 *(right side*).

The effects of C_4NH_2 on $[OAc]^-$ or HOAc on $[C_4NH_3]^+$ can be interpreted more directly from the change in chemical shifts. The downfield chemical shifts (increasing positive Δδ values) of H-1, H-2, H-3, and H-4 of the $[C_4NH_3]^+$ cation with increasing HOAc concentration (Fig. 4, left side) indicate that $[C_4NH_3]^+$ cations are involved in weaker interactions.[33] This is consistent with the formation of oligomeric $[H_{(n-1)}(OAc)_n]^-$ anions, which are weaker bases and therefore increase the cationic, electron withdrawn character of $[C_4NH_3]^+$. Among the four butyl protons, H-1 has larger chemical shifts than H-2, H-3, or H-4, as H-1 is more engaged in interactions with acetate than the other three protons. The nitrogen protons are exchangeable and not discussed here.

C_4NH_2 has a more complicated effect on $[OAc]^-$ (indicated as H-6 in Fig. 4). First, there is an upfield shift which peaks at 0.2 molar fraction C_4NH_2 and may indicate the weakening of cation-anion interactions due to the formation C_4NH_2-$[C_4NH_3]^+$ effects (Fig. 4, right side). From then on, the chemical shift of $[OAc]^-$ moves downfield, possibly because the lower concentration of $[OAc]^-$ means that hydrogen bond donors are in abundance, and it is well-solvated.

To confirm the interactions noted in the NMR data, the mixtures were further analyzed by ATR-FTIR (full spectra in Fig. S9, ESI). The discussion here focuses on the carbonyl C–O stretches (Fig. 5), which are the most diagnostic for investigating effects on ionicity. When protonated, the asymmetric stretching modes of the C–O bonds in of the $[OAc]^-$ anion (at 1534 cm^{-1} in $[C_4NH_3][OAc]$) will split into the C=O and C–O stretching modes of HOAc at 1712 and 1280 cm^{-1}, respectively.[34] In interesting contrast to the NMR and DSC, the two peaks are quite insensitive to changes in HOAc concentration. The largest changes in the position of the $[OAc]^-$ C–O asymmetric stretching band are for systems with large amounts of HOAc (0.8 and 0.9 molar fraction) and are still quite small in magnitude (Table 1). Also, the HOAc C=O stretch can be observed at all concentrations, indicating an absence of ionic character. This could indicate that, while DSC and NMR support that $[OAc]^-$ and HOAc form oligomeric species, the transfer of charge may be coupled to the slower exchange process of H^+ between the two species rather than the existence of a long-lived $[H(OAc)_2]^-$ anion with a delocalized charge.

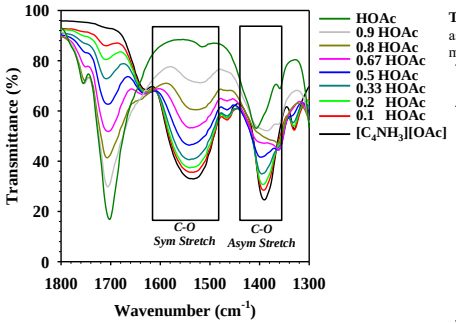

Table 1. IR frequencies of the asymmetric C–O stretch in the mixtures of $[C_4NH_3][OAc]$ + HOAc

Molar fraction of HOAc (χ)	Frequency (cm^{-1})
HOAc	-
0.9 HOAc	1521
0.8 HOAc	1528
0.67 HOAc	1541
0.5 HOAc	1541
0.33 HOAc	1542
0.2 HOAc	1541
0.1 HOAc	1541
$[C_4NH_3][OAc]$	1534

Figure 5. FTIR spectra (1800–1300 cm^{-1} region) of the mixtures of $[C_4NH_3][OAc]$ + HOAc. The symmetric C–O stretch overlaps with the HOAc peak around 1410 cm^{-1}.

The asymmetric and symmetric C–O stretches of the $[OAc]^-$ anion in the $[C_4NH_3][OAc]$ + C_4NH_2 mixtures are shown in Fig. 6. With increasing C_4NH_2 concentration, both the asymmetric and symmetric C–O stretches are blue-shifted, indicating increased hydrogen bond donation to $[OAc]^-$ anions (Fig. 6). This is in agreement with the NMR chemical shifts, which support an increase in hydrogen bonding to $[OAc]^-$ at high C_4NH_2 concentrations. The interactions between C_4NH_2 and acetate anions could also result in IR shifts of the NH_2 vibration, however, the NH_2 bending vibration[35] around 1605 cm^{-1} with low intensity overlaps with the C–O asymmetric stretch (Fig. 6a). Shifts of NH_2 are not further discussed.

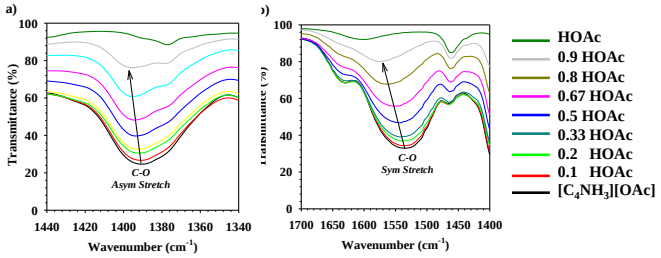

Figure 6. FT-IR spectra of the mixtures of $[C_4NH_3][OAc]$ + C_4NH_2. **a)** Asymmetric C–O stretch; **b)** Symmetric C–O stretch.

Spectroscopic data confirm the analysis based on thermal properties of the mixtures. The addition of HOAc to the system generates oligomeric ions, resulting in a compound with a much lower melting point at 1:1 IL:HOAc, consistent with making larger ions. Although the addition of C_4NH_2 to the system also appears to produce oligomeric ions, its effect is different: because $[C_4NH_3]^+$ and C_4NH_2 are capable of Grotthus proton exchange, small amounts of C_4NH_2 help the 1:1 salt crystallize while small amounts of IL inhibit the freezing of C_4NH_2. At

View Article Online
DOI: 10.1039/C7CP04078D

compositions near 1:1 the system becomes even lower melting and stops crystallizing, possibly because $[C_4NH_3]^+$-C_4NH_2 interactions are producing large, ill-defined, 3-dimensional clusters. These differences on the type of networks that are formed when HOAc and C_4NH_2 might have implication on the physical and chemical properties of the resulting mixtures, as discussed in the following sections.

Physical Properties of the Mixtures

Viscosities and densities of $[C_4NH_3][OAc]$, HOAc, C_4NH_2, and the mixtures were measured at 30 °C. The viscosity of the neat IL (which is a supercooled liquid under the measurement condition) is notably greater than that of HOAc or C_4NH_2 (Fig. 7). The high viscosity of $[C_4NH_3][OAc]$ can also be attributed to the strong electrostatic attraction and hydrogen bonding between the cation and anion.[36] Viscosities of the mixtures decrease significantly with increase of HOAc or C_4NH_2, and present concave curves as a function of the molar fraction of the acid or C_4NH_2. The viscosity behavior observed here is different from that of the *N*-methylpyrrolidine-HOAc mixtures,[14] in which the viscosity has maximum value when the molar ratio of *N*-methylpyrrolidine to HOAc is 1:2.

The experimental values in this study were compared with the values predicted by logarithmic law (eq. 2)[37] and a single exponential equation (eq. 3)[38,39]:

$$\log \eta = \chi \log \eta_A + (1-\chi) \log \eta_B \quad (2)$$

$$\eta = \eta_B \exp(-\chi/a) \quad (3)$$

where χ is the molar fraction of HOAc (or C_4NH_2), η is the viscosity of the mixtures, η_A and η_B are the viscosities of HOAc (or C_4NH_2) and $[C_4NH_3][OAc]$, respectively, and a is a constant with a value of 0.216.[39] The experimental values of the mixtures of $[C_4NH_3][OAc]$ + HOAc fit the values predicted by the exponential equation (Fig. 7, left side), while the experimental results of the $[C_4NH_3][OAc]$ + C_4NH_2 mixtures match the values calculated by the logarithmic law (Fig. 7, right side).

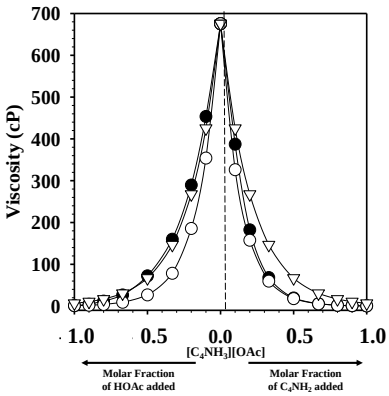

Figure 7. Viscosities of the mixtures of $[C_4NH_3][OAc]$ + HOAc *(left side)* and the mixtures of $[C_4NH_3][OAc]$ + C_4NH_2 (right side). Experimental values (●) were compared with the calculated logarithmic (○) and exponential (▽) equations.

Interactions between the species in the mixtures are different, and thus can be used to explain the differences in viscosity behaviors. The Grotthus mechanism discussed with the addition of C_4NH_2 to $[C_4NH_3][OAc]$ increases the mobility of $[C_4NH_3]^+$ ions, thus decreasing the viscosity of the system. On the other hand, formation of anionic oligomeric species with the addition of HOAc also leads to decreased interactions between $[C_4NH_3]^+$ and $[OAc]^-$, which further results in decreased viscosity of the mixture.

The density of the $[C_4NH_3][OAc]$ liquid at room temperature (0.9525 g/mL, Fig. 8) is lower than that of the crystal at 0 °C (1.086 g/mL). The difference is rather large (14% of the density of liquid $[C_4NH_3][OAc]$; for comparison, the density of ice at 0 °C *vs.* water at 25 °C diminishes by 9%). Densities of the mixtures of $[C_4NH_3][OAc]$ + HOAc increase with increasing HOAc molar fraction and reached a maximum value when χ_{HOAc} = 0.90. The formation of oligomeric anionic species at higher HOAc concentrations can result in denser packing, thus leading to higher densities of the mixtures than the neutral acid. The change is mostly linear, but there are plateaus near 100% HOAc and 100% IL that indicate a small amount of IL in HOAc or of small excess HOAc in IL can, respectively, decrease or increase the packing density. Densities of the mixtures of $[C_4NH_3][OAc]$ + C_4NH_2 decrease nonlinearly with increase of C_4NH_2 concentration. In the mixture of $[C_4NH_3][OAc]$ + C_4NH_2, the density values vary between the densities of the neat IL and the amine, indicating a decrease in the interactions between the cation and anion with increasing C_4NH_2 concentration.

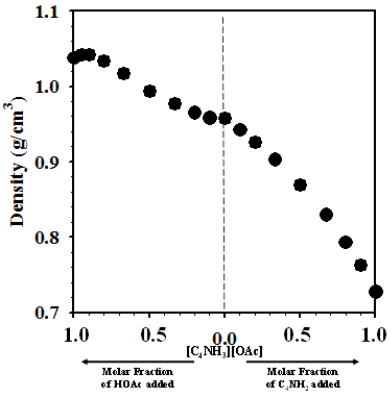

Figure 8. Densities of the mixtures of $[C_4NH_3][OAc]$ + HOAc (*left side*) and the mixtures of $[C_4NH_3][OAc]$ + C_4NH_2 (*right side*).

Excess molar volumes (V^E) of the mixtures (Fig. 9) were calculated using eq. 4:[37]

$$V^E = \frac{\chi \times M_{(A)} + (1-\chi) \times M_{(B)}}{\rho} - (\chi \times V_{M(A)} + (1-\chi) \times V_{M(B)}) \quad (4)$$

where A and B denote HOAc (or C_4NH_2) and $[C_4NH_3][OAc]$, respectively, χ is the molar fraction of A, M is the formula weight, ρ is the density of the resulting system, and V_M is the molar volume (*i.e.*, volume occupied by one mole of a substance). Excess molar volumes of all the mixtures have negative values, and V^E first decreases and then increases as the concentration of HOAc (or C_4NH_2) increases, reaching a minimum value when χ_{HOAc} = 0.67 (or χ_{C4NH2} = 0.50), molar ratios that coincide with mixtures without thermal transitions (DSC determinations). The negative V^E values of the mixtures indicate that the packing in the mixtures is more efficient, which is attributed to the strong interactions between the IL and the acid or base. Furthermore, the changing behavior of V^E as a function

View Article Online
DOI: 10.1039/C7CP04078D

of the acid or base concentration is asymmetrical, which is a typical behavior when the mixture components have a significant molar volume difference.[40] The minimum V^E values might be due to the formation of quasi-clathrates in the vicinity at $\chi = 0.67$ as suggested by Wang *et al.*[41] and Zhong *et al*.[42] in the mixtures of 1-butyl-3-methylimidazolium hexafluorophosphate and organic components.

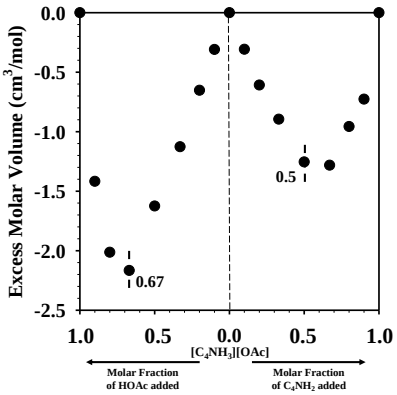

Figure 9. Excess molar volumes of the mixtures of $[C_4NH_3][OAc]$ + HOAc (*left side*) and the mixtures of $[C_4NH_3][OAc]$ + C_4NH_2 (*right side*).

Chemical Properties of the Mixtures (Solvent Properties)

Solubility of organic solutes

Organic solutes with different properties, nonpolar aromatics (benzene), nonpolar lipophilics (heptane), ether (diethyl ether), and polar aprotic (ethyl acetate), were chosen to study the solvation properties of the $[C_4NH_3][OAc]$ mixtures. The solubilities of the organics in the neat IL ($\chi_{HOAc} = 0.00$) are low (from 0.05 mole heptane to 0.93 mole benzene per mole of IL, Table S2, ESI), in comparison with their high solubility in pure HOAc ($\chi_{HOAc} = 1.00$) or C_4NH_2 ($\chi_{C4NH2} = 1.00$), where all the organic solutes are miscible except for heptane in HOAc (0.12 mol/mol HOAc).

$[C_4NH_3][OAc]$ + HOAc. With the addition of HOAc to the IL, the solubilities of ethyl acetate, benzene, and diethyl ether increased up to $\chi_{HOAc} = 0.20$, 0.20, and 0.50, respectively, after which the solutes were totally miscible with the mixtures (Table S2, ESI, and Fig. 10). (It should be noted that diethyl ether solubility increased significantly from 1.25 mol/mol mixture at $\chi_{HOAc} = 0.33$ to 8.66 mol/mol mixture at $\chi_{HOAc} = 0.50$.) The formation of $[H(OAc)_2]^-$ species might be the main factor that contributes to these drastic changes in solubility; the formation of the anionic species decreases the interactions between the cation and the anion, and thus the interactions between the cation and the organic solutes are increased. The solubility of the nonpolar, non-hydrogen-bonding heptane in the mixture of $[C_4NH_3][OAc]$ + HOAc did not change with HOAc concentration.

$[C_4NH_3][OAc]$ + C_4NH_2. Due to the high solubility of the compounds in the pure base (Table S2, ESI), the solubilities of all the four solutes increase with the addition of C_4NH_2 to the IL (Fig. 10). As discussed in the sections above, the species present in the system aren't modified with the addition of the base but the mobility of the ions in solution. With the increase of the base, a larger number of hydrogen bond acceptors can be accommodated in the solution, thus increasing the solubility of ethyl acetate, diethyl ether, and benzene. In addition, the hydrophobic alkyl change of the base interacts with the non-polar heptane. (It was previously demonstrated by our group that a C4-alkyl change is enough to interact with long, hydrophobic alkyl-chains.[11])

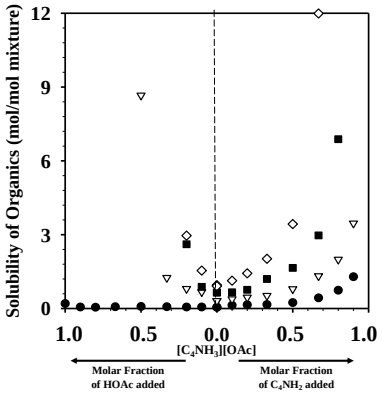

Figure 10. Solubility of ethyl acetate (■), benzene (◇), diethyl ether (▽), and heptane (●) in the mixtures of $[C_4NH_3][OAc]$ + HOAc (*left side*) and in the mixtures of $[C_4NH_3][OAc]$ + C_4NH_2 (*right side*).

Solubility of APIs

To evaluate the possibility of the use of the $[C_4NH_3][OAc]$ mixtures in the pharmaceutical industry, the ability of these to dissolve active pharmaceutical ingredients (APIs) was studied using ibuprofen free acid and lidocaine free base as model compounds. Ibuprofen solubility (Table S3, ESI) in the neat $[C_4NH_3][OAc]$ (0.15 mol/mol IL) is similar to that in HOAc (0.23 mol/mol HOAc), although its solubility in the mixtures of $[C_4NH_3][OAc]$ + HOAc (Fig. 11a) first increased significantly and then decreased with increasing HOAc concentration. Interestingly, when the moles of free acid (ibuprofen + HOAc in excess) are compared with the moles of total HOAc species present in the mixture, the solubility of the free acid reaches a maximum close to three moles of acid per mole of HOAc present in solution (1.25 ± 0.25 mole Ibu+HOAc per mole total HOAc species, Fig. 11a). Interestingly, this value is nearly constant; increasing the amount of HOAc reduces the solubility of ibuprofen. The reduced interactions between $[C_4NH_3]^+$ and $[OAc]^-$ at low HOAc concentrations will "free" the $[OAc]^-$ anions to hydrogen bond with ibuprofen, thus, increasing the solubility of this drug at low HOAc molar ratios until all $[OAc]^-$ are occupied, reaching the maximum solubility.

On the other hand, when free ibuprofen is added to the $[C_4NH_3][OAc]$ + C_4NH_2 mixtures, it is expected that ibuprofenate is formed (pKa ibuprofen: 5.4[43]), thus modifying the speciation of the API. When ibuprofen was added to pure C_4NH_2 or $[C_4NH_3][OAc]$ with excess C_4NH_2, all the systems crystallized. PXRD showed that none of the solids contained detectable amounts of ibuprofen but instead new crystalline phases (Fig. S10, ESI). One of these phases could be identified by SCXRD as $[C_4NH_2][Ibuprofenate]$, which crystallized in $P2_12_12_1$ with one unique formula unit per asymmetric unit. The $[C_4NH_3]^+$ groups engage in similar interactions with the carboxylate group of

View Article Online
DOI: 10.1039/C7CP04078D

ibuprofenate as those observed in $[C_4NH_3][OAc]$, although it can be seen in Fig. 11c that the butyl group has a different conformation, with the terminal methyl group in a gauche position. This appears to maximize overlap of the butyl chain with the ibuprofenate phenyl ring and promote additional C-H···π interactions.

An interesting feature of the structure is that the packing is chiral despite the fact that the ibuprofen used was racemic. PXRD (Fig. S11, ESI) suggests that there are additional phases present which do not match ibuprofen or the single crystal structure of $[C_4NH_3][Ibuprofenate]$, and optical polarizing microscope photographs (Fig. S12, ESI) also suggest the presence of at least two phases, larger crystalline prisms which consistently index as the $P2_12_12_1$ structure and smaller needles which could not be indexed by SCXRD. Given the lack of a driving force to explain a strictly chiral crystal system, it seems most likely that the small crystals are a racemic form of $[C_4NH_3][Ibuprofenate]$. Crystallization of $[C_4NH_3][Ibuprofenate]$ from $[C_4NH_3][OAc]$ + C_4NH_2 is likely driven by the common ion effect – the less soluble ibuprofenate ion precipitates so that the more soluble $[OAc]^-$ can remain in solution.

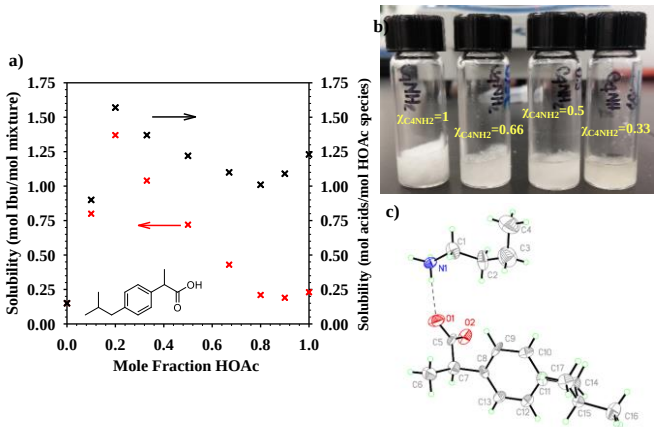

Figure 11. a) Solubility of ibuprofen in the mixtures of $[C_4NH_3][OAc]$ + HOAc, (✕) mole of ibuprofen per mole of mixture and (✕) mole of acid (ibuprofen + HOAc in excess) per mole of total HOAc species in the mixture; **b)** Solutions of ibuprofen in the mixtures of $[C_4NH_3][OAc]$ + C_4NH_2; and **c)** 50% probability ellipsoid plot of asymmetric unit of $[C_4NH_3][Ibuprofenate]$, dashed line indicates shortest contact between ions.

Lidocaine solubility is also increased with the addition of C_4NH_2 (1 mole pure $[C_4NH_3][OAc]$ can only dissolve 0.06 mole lidocaine, Table S3, ESI). As seen in Fig. 12a, lidocaine solubility is almost linear with the addition of C_4NH_2, although its solubility in mixtures with $[C_4NH_3][OAc]$ in excess is still lower than in pure base. When C_4NH_2 is in excess hydrogen bonds can be formed with lidocaine (pKa lidocaine: 7.2[44]), thus increasing the solubility of the API. However, when lidocaine is solubilized in the mixtures containing HOAc in excess, lidocaine rapidly crystallized out of the system, and no other crystalline phases were detected (Fig. 12b, and PXRD Fig. S13, ESI). It is important to remark that, although the solubility of the mixtures $[C_4NH_3][OAc]$ + HOAc is low (*e.g.*, 0.22 mole lidocaine per mole mixture), its solubility in pure HOAc is remarkably higher (1 mole lidocaine per mole HOAc), due to the formation of the already reported [Lid][OAc].[45]

The solubility of the four organic solutes and the APIs evidences the different interaction and species that occur upon the addition the acid and the base; while the addition of the acid drastically modifies the solubility of the compounds due to the formation of new species, the addition of the base modifies the mobility of the ions and the interactions with the solutes, although not the speciation. This major difference results in a higher tunability of the solubility of the solutes with the addition of C_4NH_2 than with the addition of HOAc. In addition, the solubility of APIs in the mixtures open a novel option for crystallization of pure acid and basic APIs with the sole modification of the composition of the mixtures.

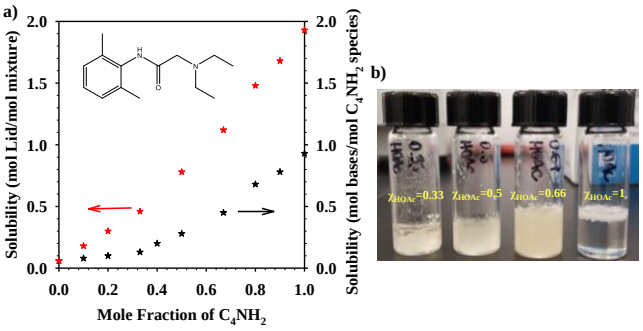

Figure 12. a) Solubility of lidocaine in the mixtures of $[C_4NH_3][OAc]$ + C_4NH_2, (★) mole of lidocaine per mole of mixture, and (★) mole of bases (lidocaine + C_4NH_2 in excess) per total mole of C_4NH_2 in the mixture; and **b)** Solutions of lidocaine in the mixtures of $[C_4NH_3][OAc]$ + HOAc.

Conclusions

In the present work, we have shown that the addition of corresponding parent acid or base to a protic ionic liquid composed by a primary amine as a base and a carboxylic acid results in systems with different behavior due to the different interactions occurring. Using thermal and spectroscopic data, we were able to show the specific interactions between the species in the mixtures, which help to understand the different behaviors of the mixtures.

The addition of HOAc to the IL induces the formation of new anionic species, *e.g.*, $[H(OAc)_2]^-$, resulting in a compound with a much lower melting point at 1:1 IL:HOAc, consistent with making larger ions. On the other hand, the addition of C_4NH_3 to the IL also appears to produce oligomeric ions, but by an effect we do not think has been explored in ILs before: The $[C_4NH_3]^+$-C_4NH_2 interactions induce the formation of large clusters, which modify the crystallization points of C_4NH_2 and the IL.

These differences in interactions resulted in tunable properties, including viscosity, density, and dissolving power. Solubilities of benzene, ethyl acetate, and diethyl ether in the $[C_4NH_3][OAc]$ and HOAc mixtures, as well as the C_4NH_2 mixtures increase with increase of HOAc or C_4NH_2 concentration, although their solubilities in the acidic mixtures can only be varied with low concentrations of HOAc. On the other hand, heptane could not be dissolved in the protic IL and HOAc mixtures, and its solubility in the $[C_4NH_3][OAc]$ and amine mixtures increases smoothly with amine content.

Although neither the IL nor HOAc is a good solvent to dissolve ibuprofen (in its free acid form), its solubility increases in mixtures of $[C_4NH_3][OAc]$ and HOAc. Likewise, the solubility of free lidocaine in the $[C_4NH_3][OAc]$ and C_4NH_2 mixtures increases with the amine molar fraction, likely by weakening the strength of C_4NH_2 as an hydrogen-bond donor. Interestingly, the addition of an acid API, such as ibuprofen, to a mixture with excess of C_4NH_2 induces the crystallization of the API as a $[C_4NH_3]^+$ salt while the addition of lidocaine, the free base of the API, to mixtures with excess of HOAc induces crystallization of the API in its pure form.

All in all, this study illustrates that adding an acid or a base to a protic IL can result in ion oligomerization and thus change the speciation in the system, leading to solvents with tunable physicochemical properties, useful for many industrial processes. The nature of this change is flexible, as the ions tend to interact with their conjugate acid or base selectively to produce different types of oligomeric ions depending on what is added. In particular, the synthesis and purification of APIs in pharmaceutical processes might be benefit by these tunable solvents, allowing the solubilization and crystallization of pure APIs with only two chemicals, solely by controlling their ratio.

Acknowledgements

We thank the Novartis-Massachusetts Institute of Technology (MIT) Center for Continuous Manufacturing (CCM) and Novartis International AG for financial support. This research was undertaken, in part, thanks to funding from the Canada Excellence Research Chairs Program.

Notes and references

1 R. Hayes, G. G. Warr and R. Atkin, *Chem. Rev.*, 2015, **115**, 6357.
2 J. G. Huddleston, A. E. Visser, W. M. Reichert, H. D. Willauer, G. A. Broker and R. D. Rogers, *Green Chem.*, 2001, **3**, 156.
3 H. Rodríguez, Ed. *Ionic Liquids for Better Separation Processes*, Springer-Verlag Berlin Heidelberg, Heidelberg, 2016.
4 H. Niedermeyer, J. P. Hallett, I. J. Villar-Garcia, P. A. Hunt and T. Welton, *Chem. Soc. Rev.*, 2012, **41**, 7780.
5 A. B. Pereiro, J. M. M. Araújo, F. S. Oliveira, C. E. S. Bernardes, J. M. S. S. Esperança, J. N. C. Lopes, I. M. Marrucho and L. P. N. Rebelo, *Chem. Commun.*, 2012, **48**, 3656.
6 M. Y. Lui, L. Crowhurst, J. P. Hallett, P. A. Hunt, H. Niedermeyer and T. Welton, *Chem. Sci.*, 2011, **2**, 1491.
7 M. Smiglak, N. J. Bridges, M. Dilip and R. D. Rogers, *Chem. Eur. J.*, 2008, **14**, 11314.
8 G. Chatel, J. F. B. Pereira, V. Debbeti, H. Wang and R. D. Rogers, *Green Chem.*, 2014, **16**, 2051.
9 H. Wang, J. F. B. Pereira, A. S. Myerson and R. D. Rogers, *ECS Trans.*, 2014, **64**, 33.
10 H. Wang, S. P. Kelley, J. W. Brantley, G. Chatel, J. Shamshina, J. F. B. Pereira, V. Debbeti, A. S. Myerson and R. D. Rogers, *ChemPhysChem*, 2015, **16**, 993.
11 H. Wang, P. Berton, A. S. Myerson and R. D. Rogers, *ECS Trans.*, 2016, **75**, 451.
12 J. Wang, T. L. Greaves, D. F. Kennedy, A. Weerawardena, G. Song and C. J. Drummond, *Aust. J. Chem.*, 2011, **64**, 180.
13 T. L. Greaves and C. J. Drummond, *Chem. Rev.*, 2008, **108**, 206.
14 K. M. Johansson, E. I. Izgorodina, M. Forsyth, D. R. MacFarlane and K. R. Seddon, *Phys. Chem. Chem. Phys.*, 2008, **10**, 2972.
15 K. Bica and R. D. Rogers, *Chem. Commun.*, 2010, **46**, 1215.
16 G. J. Maximo, R. J. B. N. Santos, J. A. Lopes-da-Silva, M. C. Costa, A. J. A. Meirelles and J. A. P. Coutinho, *ACS Sustainable Chem. Eng.*, 2014, **2**, 672.
17 M. S. Miran, H. Kinoshita, T. Yasuda, Md. A. B. H. Susan and M. Watanabe, *Phys. Chem. Chem. Phys.*, 2012, **14**, 5178.
18 B. Nuthaki, T. L. Greaves, I. Krodkiewska, A. Weerwardena, M. I. Burgar, R. J. Mulder and C. J. Drummond, *Aust. J. Chem.*, 2007, **60**, 21.
19 M. Shen, Y. Zhang, K. Chen, S. Che, J. Yao and H. Li, *J. Phys. Chem. B*, 2017, **121**, 1372.
20 M. Yoshizawa, W. Xu and C. A. Angell, *J. Am. Chem. Soc.*, 2003, **125**, 15411.
21 P. D. McCrary, P. A. Beasley, G. Gurau, A. Narita, P. S. Barber, O. A. Cojocaru and R. D. Rogers, *New J. Chem.*, 2013, **37**, 2196.
22 Apex3, version 2015-R7, Bruker-AXS: Madison, WI, 2015 (Accessed 04/22/2017).
23 SADABS, An Empirical Absorption Correction Program, v.2.01., Bruker AXS Inc., Madison, WI, 2001.
24 G. M. Sheldrick, SHELXTL, Structure Determination Software Suite, v.6.10., Bruker AXS Inc., Madison, WI, 2001.
25 C. F. Macrae, I. J. Bruno, J. A. Chisholm, P. R. Edgington, P. McCabe, E. Pidcock, L. Rodriguez-Monge, R. Taylor, J. van de Streek and P. A. Wood, *J. Appl. Crystallogr.*, 2008, **41**, 466.
26 M. Lin, M. Tesconi and M. Tischler, *Int. J. Pharm.*, 2009, **369**, 47.
27 M. Yoshizawa, W. Xu and C. A. Angell, *J. Am. Chem. Soc.*, 2003, **125**, 15411.
28 S. P. Kelley, A. Narita, J. D. Holbrey, K. D. Green, W. M. Reichert and R. D. Rogers, *Cryst. Growth Des.*, 2013, **13**, 965.
29 Y. Fukaya, Y. Iizuka, K. Sekikawa and H. Ohno, *Green Chem.*, 2007, **9**, 1155.
30 S. Fendt, S. Padmanabhan, H. W. Blanch and J. M. Prausnitz, *J. Chem. Eng. Data*, 2011, **56**, 31.
31 A. P. Abbott, D. Boothby, G. Capper, D. L. Davies and R. K. Rasheed, *J. Am. Chem. Soc.*, 2004, **126**, 9142.
32 G. Gurau, H. Rodríguez, S. P. Kelley, P. Janiczek, R. S. Kalb and R. D. Rogers, *Angew. Chem. Int. Ed.*, 2011, **50**, 12024.
33 A. D. Headley and N. M. Jackson, *J. Phys. Org. Chem.*, 2002, **15**, 52.
34 F. Quils and A. Burneau, *Vib. Spectrosc.*, 1998, **16**, 105.
35 T. Morimoto, J. Imai and M. Nagao, *J. Phys. Chem.*, 1974, **78**, 704.
36 Y. Geng, T. Wang, D. Yu, C. Peng, H. Liu and Y. Hu, *Chinese J. Chem. Eng.*, 2008, **16**, 256.
37 G. Annat, M. Forsyth and D. R. MacFarlane, *J. Phys. Chem. B*, 2012, **116**, 8251.
38 K. R. Seddon, A. Stark and M.-J. Torres, *Pure Appl. Chem.*, 2000, **72**, 2275.
39 J. Wang, Y. Tian, Y. Zhao and K. Zhuo, *Green Chem.*, 2003, **5**, 618.
40 M. Geppert-Rybczyńska, J. K. Lehmann and A. Heintz, *J. Chem. Thermodyn.*, 2014, **71**, 171.
41 J. Wang, A. Zhu, Y. Zhao and K. Zhuo, *J. Solution Chem.*, 2005, **34**, 585.
42 Y. Zhong, H. Wang and K. Diao, *J. Chem. Thermodyn.*, 2007, **39**, 291.
43 U. Domańska, A. Pobudkowska, A. Pelczarska and P. Gierycz, *J. Phys. Chem. B*, 2009, **113**, 8941.
44 H. Sjöberg, K. Karami, P. Beronius and L.-O. Sundelöf, *Int. J. Pharm.*, 1996, **141**, 63.
45 Z. Wojnarowska, K. J. Paluch, E. Shoifet, C. Schick, L. Tajber, J. Knapik, P. Wlodarczyk, K. Grzybowska, S. Hensel-Bielowka, S. P. Verevkin and M. Paluch, *J. Am. Chem. Soc.*, 2015, **137**, 1157.